CARRIER BASED PWM TECHNIQUE AND ADAPTIVE NEURAL NETWORK BASED ROTOR RESISTANCE ESTIMATOR FOR THE PERFORMANCE ENHANCEMENT OF VECTOR CONTROLLED INDUCTION MOTOR DRIVES

A. Venkadesan

Department of Electrical and Electronics Engineering, National Institute of Technology Puducherry, Thiruvettakudy, karaikal-609609, India.

ABSTRACT: In this paper, the carrier based Pulse Width Modulation (PWM) technique and neural network based rotor resistance estimator are proposed for vector controller Induction motor (IM) drives. The popular sine PWM is used for induction motor drive. The popular sine PWM has poor harmonic profile and (DC) utilization. The space vector modulation (SVM) technique overcomes the disadvantages of sine PWM. But SVM is computationally complex. Hence a simple PWM technique namely "carrier based PWM technique" similar to SVM is identified and proposed for vector controlled IM drive. The experimental set up is built up and the performance of carrier based PWM is validated using FPGA processor. The adaptive neural network based rotor resistance estimator in predictive mode is proposed for the vector controlled induction motor drive. The performance enhancement of the drive with carrier based PWM and rotor resistance estimator is comprehensively presented.

تقنية تعديل عرض النبضة القائمة على الناقل ومقدار مقاومة الدوران القائم على الشبكة العصبية التكيفية من أجل تحسين الأداء للمحركات الحثية موجهة التحكم

أ. فينكاديسان

الملخص: قمنا باقتراح تعديل عرض النبضة القائمة على الناقل مقاوم الدوران القائم على الشبكة العصبية التكيفية للمحركات الحثية موجهة التحكم. ويتسم جيب زاوية جهاز تعديل عرض النبضة بسمة توافقية ضعيفة عند استخدام التيار المباشر. ويعمل استخدام تقنية تعديل اتجاه النطاق على التغلب على عيوب جيب زاوية تعديل عرض النبضة. لكن يُتعد تقنية تعديل اتجاه النطاق أمرا معقدا من الناحية الحسابية. ومن ثم ، قمنا بتحديد تقنية بسيطة لتعديل عرض النبضة وهي "تقنية تعديل عرض النبضة القائمة على الناقل المشابهة لتقنية تعديل اتجاه النطاق، واقترحنا محرك حثي قابل للتحكم فيه. و قمنا بإعداد التركيب التجريبي والتحقق من مدى صحة أداء ناقل الحركة القائم على تقنية تعديل اتجاه الحركة باستخدام معالج تنسيق قابل للبرمجة لنطاق المدخل. ونقترح استخدام تقنية مقاومة الدوران القائم على الشبكة العصبية التكيفية في الوضع التنبئي للمحركات الحثية موجهة التحكم. و عملنا على عرض شامل لمقدار تحسين الأداء للمحركات الحثية موجهة التحكم مع تعديل عرض النبضة القائم على الناقل ومقدّر مقاومة الدوران.

Corresponding author's e-mail: venkadesan@nitpy.ac.in

NOMENCLATURE

v_{ds}^s, v_{qs}^s	- d-axis Stator voltage, q-axis Stator voltage
i_{ds}^s, i_{qs}^s	- d-axis Stator current, q-axis Stator current
$\varphi_{dr}^s, \varphi_{qr}^s$	- d-axis Rotor flux, q-axis Rotor flux
R_S, R_r	- Stator resistance, Rotor Resistance
L_S, L_r	- Stator inductance, rotor inductance
L_m	- Magnetization inductance
T_s	- Sampling Time
ω_r	- Rotor Speed (rad/sec)
Superscript s	- Stationary Reference Frame
Superscript e	- Synchronous Reference Frame

1. INTRODUCTION

Three phase induction motor drives are popularly employed for variable speed control applications in many industries. This is due to their ease in maintenance (Abdelkarim Ammar *et al.* 2017; Ahmed A.Z. Diab 2014; Venkadesan A *et al.* 2016; Venkadesan A *et al.* 2017; Witold Pawlus *et al.* 2017). Now-a-days, for high performance applications, vector control provides good alternative as compared to scalar control methods. Various pulse width modulation techniques are used to generate pulse for three phase inverter in vector controlled IM drives. Out of which, space vector modulation technique (Benchabane *et al.* 2012; Bimal K. Bose 2005; Durgasukumar G *et al.* 2012; Govindasamy *et al.* 2014; Hannan M. A *et al.* 2017; Mahmoud Gaballah *et al.* 2013; Sabah V.S *et al.* 2015) is attaining popularity because it has the advantages of having better DC utilization and better harmonic profile as compared to sine-PWM technique. The space vector modulation technique is computationally rigorous and complex as it involves many mathematical calculations (Govindasamy *et al.* 2014; Hannan M.A *et al.* 2017; Sabah V.S *et al.* 2015). The carrier based PWM technique with a common mode voltage injection method is proposed for a three phase inverter Keliang Zhou *et al.* 2002). In the paper by Keliang Zhou *et al.* (2002), it is mathematically proved that the carrier based PWM technique with the common mode voltage injection method performs similar to SVM technique. But the carrier based PWM technique is simple for on-line digital implementation. In the paper Keliang Zhou *et al.* (2002), the application of the technique is not demonstrated in vector controlled IM drives. The same technique is proposed for open loop speed control of multilevel inverter fed permanent magnet motor Shriwastava R.G *et al.* (2016) and not demonstrated in vector controlled IM drives.

In this paper, the same technique is proposed for

vector controlled IM drive. The proposed carrier based PWM technique with the common mode voltage injection method technique (CB-PWM-CMV) is also implemented in FPGA (SPARTAN 6 board). The performance of CB-PWM-CMV is also validated experimentally. The vector control especially indirect type, is sensitive to rotor resistance variation (Chitra A *et al.* 2015; Karanayil B *et al.* 2007). Hence, rotor resistance estimation using a neural network approach is proposed to track variation in the rotor resistance. The neural network based rotor resistance estimator is proposed for sine PWM based vector controlled IM drive Chitra A *et al.* (2015). In the proposed work, neural network based rotor resistance estimator is proposed for CB-PWM-CMV based vector controlled IM drive. Also in the paper (Chitra A *et al.* 2015; Karanayil B *et al.* 2007), the adaptive NN is used in simulation mode. But the proposed Adaptive NN based rotor resistance estimator is used in predictive mode. The idea of using adaptive NN in predictive mode is inspired from the speed estimator proposed by Maurizio Cirrincione *et al.* (2005). In the paper by Maurizio Cirrincione *et al.* (2005), it is applied for speed estimation. In this proposed work, it is applied for rotor resistance estimation which is novel in this paper.

2. VECTOR CONTROLLED IM DRIVE

The vector control is preferred for high performance applications. The advantages of vector control are well presented in Krishnan R (2007). The indirect vector controlled IM drive with proposed PWM technique (CB-PWM-CMV) and rotor resistance estimator is shown in Fig. 1. For closed operation, the actual speed is compared with the reference speed. The speed error is processed through the PI controller. The torque
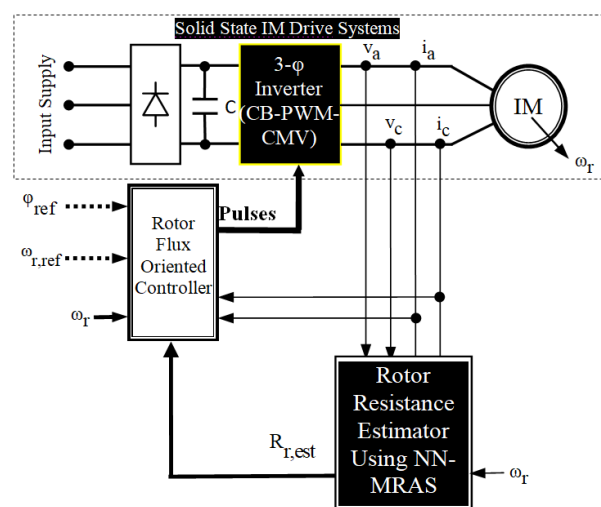
Figure 1. Indirect Vector Controlled IM Drive showing the Rotor Resistance Estimator.

command (T_e*) is generated. The reference flux producing component of current (i_d^{e*}) is generated from the reference flux (φ_{ref}) using equation (1). The reference torque producing component of current (i_q^{e*}) is generated using the equation (2). The slip frequency (ω_{sl}) is obtained using equation (3). The transformation angle (θ_e) is obtained using the equation (4). The actual three phase stator current is transformed to actual flux producing component (i_d^e) and actual torque producing component (i_q^e). The (i_d^e) is compared with (i_d^{e*})and (i_q^e) is compared with (i_q^{e*}) to produce the corresponding command voltage (V_d*, V_q*). The reference three phase voltage (V_a*, V_b*, V_c*) is generated using the command voltage and transformation angle through d-q transformation theory. The three phase duty cycle profiles are generated using the CB-PWM-CMV. The duty cycle profile/control signal is compared with the triangular signal to generate the switching pulses to the inverter.

$$i_d^{e*} = \frac{\varphi_{ref}}{L_m} \tag{1}$$

$$i_q^{e*} = \frac{4}{3p}\left[\frac{L_r T_e*}{L_m \varphi_{ref}}\right] \tag{2}$$

$$\omega_{sl} = \frac{i_q^{e*}R_r}{i_d^{e*}L_r} \tag{3}$$

$$\theta_e = \int(\omega_{sl}+\omega_r)dt \tag{4}$$

2.1 Carrier Based PWM With Common Mode Voltage Injection Technique

In the carrier based PWM with the common mode voltage injection technique, the common mode voltage is injected into the fundamental sinusoidal reference signal. The resultant signal is used as the modulating signal and it is compared with the carrier signal for the generation of switching pulses to the inverter. The addition of the common mode voltage provides lower harmonic distortion, higher fundamental output voltage Srirattanawichaikul W *et al.* (2011). The common mode voltage can be generated using three phase sinusoidal reference voltages as (5). The duty cycle for each phase can be generated using (6).

$$v_{CMV}* = -\frac{\text{Max}\left(v_a*,v_b*,v_c*\right)+\text{Min}\left(v_a*,v_b*,v_c*\right)}{2} \tag{5}$$

$$D_P = v_P* + v_{CMV}* \, , \, P \in \{a,b,c\} \tag{6}$$

$$v_a* = m_a \sin(\omega t) \tag{7}$$

$$v_b* = m_a \sin\left(\omega t - \frac{2\pi}{3}\right) \tag{8}$$

$$v_c* = m_a \sin\left(\omega t + \frac{2\pi}{3}\right) \tag{9}$$

Where m_a is the modulation index. The range of m_a is $0 < m_a \leq 1$ for under modulation ranges. The Fig. 2 shows the block diagram for the extraction of the duty cycle profile. The equations involve only simple arithmetic operations. The equations are simple, less complex and give ease in digital implementation. The Fig. 3 presents the duty cycle profile of CB-PWM-CMV.
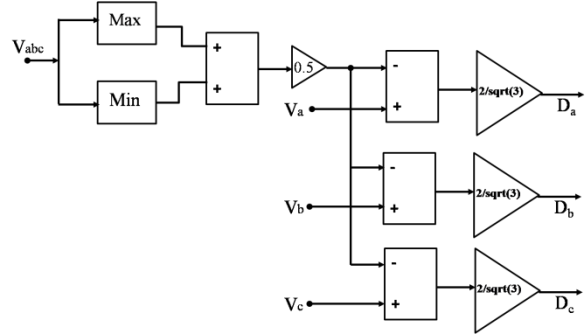
Figure 2. Duty Cycle profile Generation using CB-PWM-CMV Technique.

The performance of the proposed CB-PWM-CMV technique is compared with the SVM and Sine PWM technique in terms of DC bus utilization, harmonics profile, efficiency and complexity. The motor is operated with m=0.9, frequency=50Hz under a rated load condition. The performance comparison is shown in the Table 1.

Table 1. Comparison of CB-PWM-CMV with Sine PWM and SVM.

V_{DC} (volts)	Method	Output Voltage $V_{fundamental}$ (volts)	Output Voltage V_{THD} (%)	% Efficiency	Computational complexity
582.5	Sine PWM	455.6	79.10%	78.20%	Simple
	SVM	528	63.68%	83.43%	Complex
	CB-PWM-CMV	528	63.68%	83.43%	Simpler than SVM
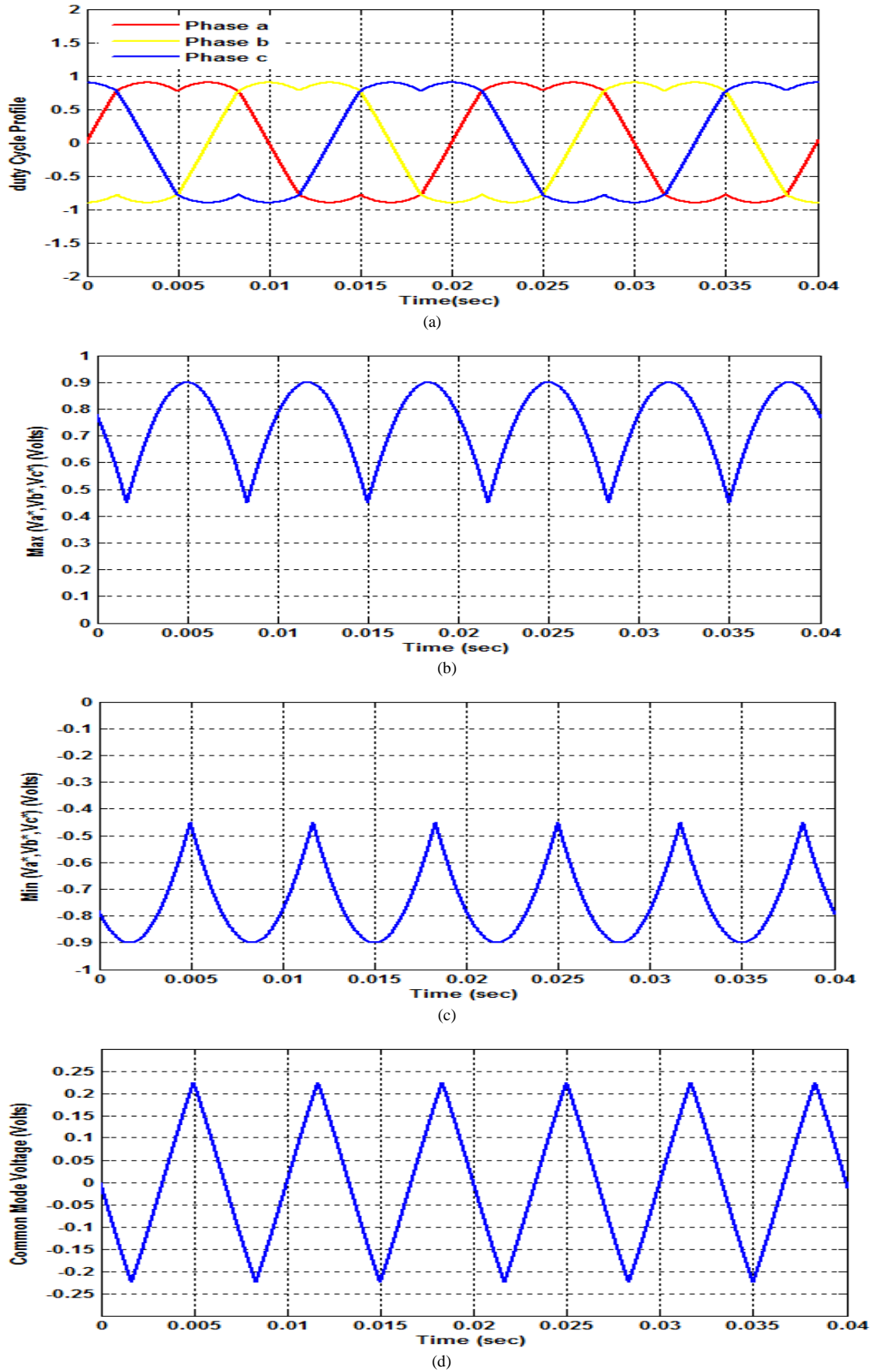
Figure 3. (a) Duty cycle profile of CB-PWM-CMV (b) Max(Va, Vb, Vc) (c) Min(Va, Vb, Vc) (d) Common mode voltage.

The Sine PWM is simple, but has poor DC bus utilization and harmonic profile. The SVM has better DC bus utilization of 15.89% as compared to sine PWM. It has an output voltage THD of 63.69% which is lesser as compared to sine PWM. The efficiency of the drive with SVM and Sine PWM is also computed in Table 1. For efficiency calculation, the electrical input power of the drive is computed using discrete 3-phase Positive-Sequence Active and Reactive Power block in MATLAB Simulink. It is seen that the efficiency of the drive is improved with SVM as compared to the drive with sine PWM. But conventional SVM is computationally complex which involves many sector calculations. The proposed CB-PWM-CMV shows a similar performance as that of SVM but it is simple and less complex. Hence, the proposed PWM technique has better DC bus utilization, a better harmonic profile and a better efficiency. Besides, it is computationally simple and offers easy on-line digital implementation.

The experimental set up is built up to validate the performance of CB-PWM-CMV. The prototype Laboratory setup is shown in Fig. 4. The CB-PWM-CMV is implemented on Spartan-6 FPGA board. The clock frequency for FPGA implementation is chosen as 20MHz. The reference sinusoidal signals are stored in a look up table with 8-bits precision as an integer. The duty cycle profiles are generated with 8-bits precision from the reference sine signals using the proposed CB-PWM-CMV technique. The VHDL coding is developed to realize the CB-PWM-CMV.

The gate pulses are given to the three phase inverter through the pulse driver circuit and opto-isolator to drive the induction motor. The switching is chosen as 10kHz. The single phase bridge rectifier [DB107], Buffer IC [CD4081], Opto-isolator [6N137] are used for hardware implementation. Two coupling capacitors of 330 µF connected in parallel (equivalent capacitor value is 660 µF) are used. The dead time for the inverter is chosen as 6µs.

The performance of CB-PWM-CMV fed induction drive is tested for various operating conditions. The sample results obtained are presented. The modulating waveform and switching pulses obtained from the FPGA processor are shown in Fig. 5(a) and Fig. 5(b) respectively. The inverter output voltage obtained for modulation index=0.96 and frequency=50Hz is shown in Fig. 6(a). The inverter output voltage obtained for modulation index=0.48 and frequency=25Hz is shown in Fig. 6(b).

The two-level inverter is used in this paper. Hence, two levels are obtained in the output line-line voltage. It is observed that as soon as the ratio of m/f is reduced to 50%, the fundamental output voltage magnitude and frequency of the line-line voltage is also reduced to around 50%. The effect of variation in the fundamental output voltage magnitude and frequency for various m/f ratios is reflected in the rotor speed. Since the rotor speed can be easily measured using tachometer, the rotor speed for various m/f ratios is shown in Table 2. The measured speed increases proportionally with increase in m/f ratio. From this table, it is shown that the drive performs very well under a practical condition with CB-PWM-CMV for various m/f ratios.
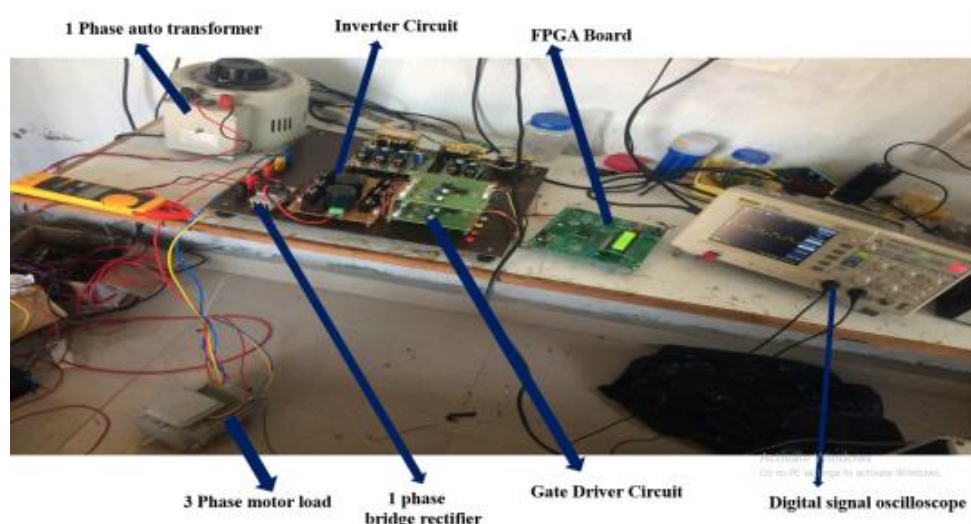
Figure 4. Hardware setup of SVM based inverter fed IM drive with FPGA controller.

(a)

(b)
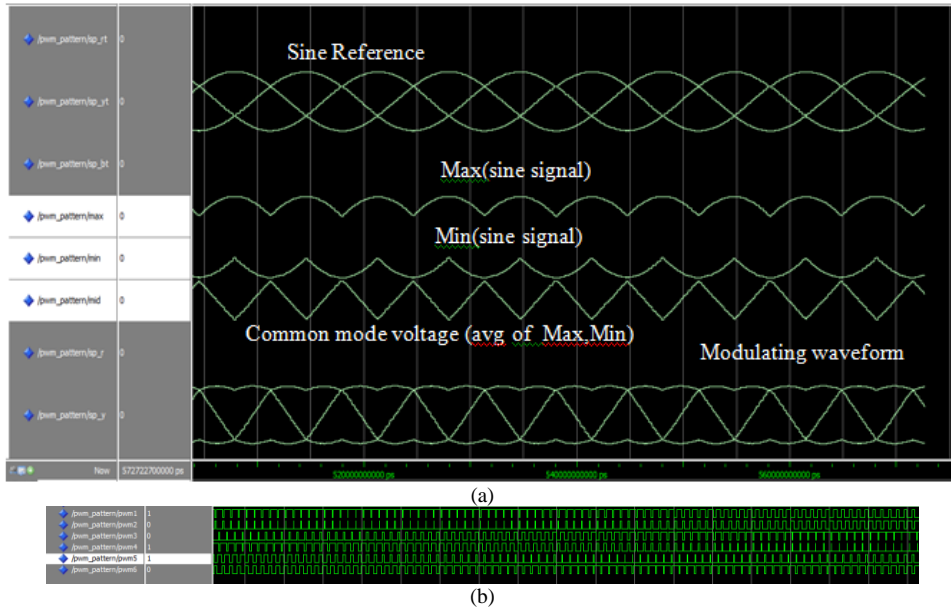
Figure 5. (a) Modulating waveform (b) Pulses to IGBT switches.

(a)

(b)

Figure 6. (a) Inverter output voltage (L-L) for m=0.96,f =50 Hz (b) Inverter output (L-L) for m=0.48, f=25 Hz.

2.2 *Adaptive Neural Network Based Rotor Resistance Estimator*

The design of an indirect vector controller, to a large extent, depends on the accuracy of the rotor resistance. The slip frequency depends on the knowledge of rotor resistance which is evident from (3). The transformation angle or flux angle depends on the slip frequency which is evident from (4). In real time, the rotor resistance may vary up to 100 due to the rotor heating Karanayil B *et al.* (2007). Any mismatch between the rotor resistance of motor and the rotor resistance value in the vector controller leads to the loss of the decoupled control (Chitra A *et al.* 2015; Karanayil B *et al.* 2007). Hence to track variation in the rotor resistance, the rotor resistance estimator using Model Reference Adaptive system (MRAS) with adaptive neural network scheme is proposed. For simulation study, the motor is modeled in d-q frame to introduce variation in the rotor resistance.

The proposed MRAS scheme for rotor resistance estimation is shown in Fig. 7. The MRAS uses a voltage and a current model for rotor resistance estimation. The output from both models is d and q-axis rotor fluxes in stationary reference frame. It is well known that the voltage model is independent of rotor resistance and the flux estimated will be independent of the rotor resistance. Hence, the voltage model is used as a reference model. Accordingly, the equations (10) and (11) do not contain rotor resistance. The three phase voltages and currents are measured and transformed into d and q axis stationary reference frame and given as inputs to the voltage model.

The current model is dependent on the rotor resistance and the flux estimated will be dependent on the rotor resistance. Therefore, the current model equation can be used as the adaptive model. Consequently, the equations (12) and (13) contain rotor resistance. The three currents and rotor speed are measured. The three phase currents are transformed into d and q axis stationary reference frame. As a result, the inputs to the current model are d and q axis current and rotor speed.

The current model equations (12), (13) are represented as a two-layer neural model and used as the adaptive model because it is dependent on the rotor resistance. The weight of the adaptive NN model

Table 2. Measured Rotor speed with CB-PWM-CMV technique for various m/f ratios.

Modulation Index	Frequency (Hz)	Measured Rotor Speed (RPM)
0.96	50	1478
0.768	40	1176
0.48	25	743
0.325	16.93	498

is the function of the rotor resistance (R_r). The error between the reference model flux and the adaptive model flux is back propagated to adjust the weights of the adaptive model to estimate the rotor resistance. The error between the reference and adaptive model is minimized using the BPM (Back Propagation with Momentum Algorithm).

$$\varphi_{dr}^s = \frac{L_r}{L_m}\left[\int (v_{ds}^s - R_s i_{ds}^s)dt\right] - \frac{L_r}{L_m}\left[\left(\frac{L_s^2 L_r - L_s L_m^2}{L_r L_s}\right)i_{ds}^s\right] \quad (10)$$

$$\varphi_{qr}^s = \frac{L_r}{L_m}\left[\int (v_{qs}^s - R_s i_{qs}^s)dt\right] - \frac{L_r}{L_m}\left[\left(\frac{L_s^2 L_r - L_s L_m^2}{L_r L_s}\right)i_{qs}^s\right] \quad (11)$$

$$\frac{\varphi_{dr}^s}{dt} = \frac{R_r L_m}{L_r}i_{ds}^s - \frac{R_r}{L_r}\varphi_{dr}^s - \omega_r \varphi_{qr}^s \quad (12)$$

$$\frac{\varphi_{qr}^s}{dt} = \frac{R_r L_m}{L_r}i_{qs}^s - \frac{R_r}{L_r}\varphi_{qr}^s + \omega_r \varphi_{dr}^s \quad (13)$$

The discrete form of Current model equations can be obtained using backward Euler's rule. Using this rule, the rate of change of rotor flux can be expressed as in (14)

$$\frac{\varphi_{dr}^s}{dt} = \frac{\varphi_{dr}^{'s}(T) - \varphi_{dr}^{'s}(T-1)}{T_s} \quad (14)$$

The discrete form of Current model equations can be obtained using backward Euler's rule and are given in (14) and (15)

$$\varphi_{dr}^{'s}(T) = W_1 \varphi_{dr}^{'s}(T-1) - W_2 \varphi_{qr}^{'s}(T-1) + W_3 i_{ds}^s(T-1) \quad (15)$$

$$\varphi_{qr}^{'s}(T) = W_1 \varphi_{qr}^{'s}(T-1) + W_2 \varphi_{dr}^{'s}(T-1) + W_3 i_{qs}^s(T-1) \quad (16)$$

Equations (14) and (15) can be represented as a two-layer neural network with a linear activation function (Fig. 8). This is used as the adaptive model. It contains four inputs { $\varphi_{dr}^{'s}(T-1)$, $\varphi_{qr}^{'s}(T-1)$, $i_{ds}^s(T-1)$, $i_{qs}^s(T-1)$ } and two outputs { $\varphi_{dr}^{'s}(T)$, $\varphi_{qr}^{'s}(T)$ }. The adaptive model is used in a predictive mode instead in simulation mode. In predictive mode. In the predictive mode, the past values of rotor flux required as the input for the adaptive model is obtained from the reference voltage model itself rather than from the adaptive model as in simulation mode. This gives ease in digital implementation of the adaptive model and overcomes the problem of instability Maurizio Cirrincione *et al.* (2005). The inputs and outputs are connected through the weights w_1, w_2, w_3. The weight w_2 is kept constant. The other two weights w_1 and w_3 are proportional to the R_r they are updated using BPM

to minimize the error E (17).

The BPM is coded in MATLAB-m-file. The learning rate (α) and momentum factor (η) are chosen as 5×10^{-5} and 2×10^{-5} respectively. The E is chosen as 1×10^{-6}. The weights of NN are updated using (20) and (21).

$$E=\frac{1}{2}\left[\varepsilon(T)\right]^2=0.5\left[\varphi_r^S(T)-\varphi_r^{'S}(T)\right]^2 \qquad (17)$$

$$\Delta w_1(T) = \alpha\left[\varepsilon_d(T)\,\varphi_{dr}^S(T-1) + \varepsilon_q(T)\,\varphi_{qr}^S(T-1)\right] \qquad (18)$$

$$\Delta w_3(T) = \left[\varepsilon_d(T)\,i_{ds}^S(T-1) + \varepsilon_q(t)\,i_{qs}^S(T-1)\right] \qquad (19)$$

$$w_1(T)=w_1(T-1)+\alpha\,\Delta w_1(T)+\eta\,\Delta w_1(T-1) \qquad (20)$$

$$w_3(T)=w_3(T-1)+\alpha\,\Delta w_3(T)+\eta\,\Delta w_3(T-1) \qquad (21)$$

where,

$$\varphi_r^S(T)=\begin{bmatrix}\varphi_{dr}^S(T)\\\varphi_{qr}^S(T)\end{bmatrix};\quad \varphi_r^{'S}(T)=\begin{bmatrix}\varphi_{dr}^{'S}(T)\\\varphi_{qr}^{'S}(T)\end{bmatrix};$$

$$\varepsilon_d(T)=\varphi_{dr}^S(T)-\varphi_{dr}^{'S}(T)\;;\;\varepsilon_q(T)=\varphi_{qr}^S(T)-\varphi_{qr}^{'S}(T)$$

The rotor resistance can be obtained either from w_1 or w_3 (Chitra A *et al.* 2015; Karanayil B *et al.* 2007).

$$R_r = \left(\frac{L_r\,w_3}{L_m\,T_s}\right) \qquad (22)$$

$$R_r = \frac{L_r}{T_s}\left(1-w_1\right) \qquad (23)$$

The effect of sampling time on the performance of the proposed rotor resistance estimator assumes importance for on-line digital implementation. Hence, the same is tested for various sampling time. The drive is operated with the speed of 148 rad/s under 100% load torque. The rotor resistance is increased to 50%. The switching frequency of the inverter is chosen as 10kHz. Hence the switching time is 100μs.
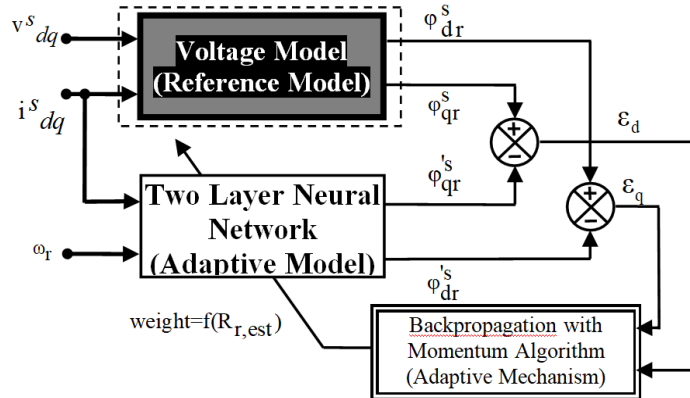
Figure 7. NN-MRAS scheme for rotor resistance estimation.
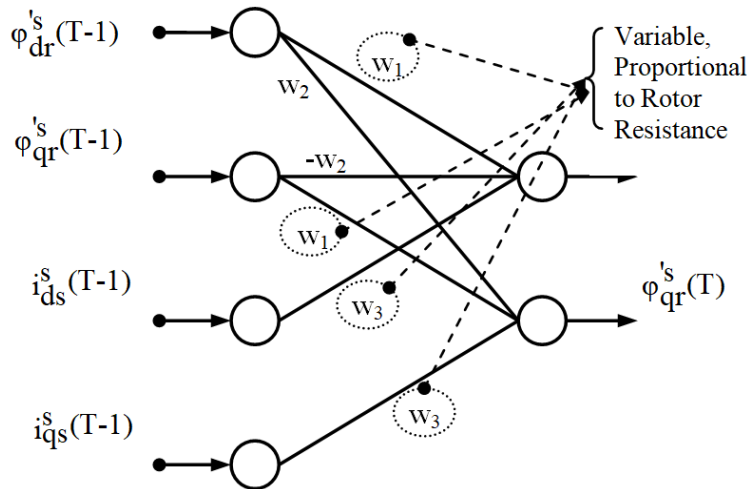
Figure 8. Two-layer neural network.

The steady state error is computed between the actual and estimated rotor resistance for various sampling time and presented in Table 3. Lesser sampling time leads to more accuracy but increases computation time as the number of samples per cycle is more. On the other hand, larger sampling time decreases computation time but it decreases accuracy as the number of samples per cycle is less. In this paper, the sampling time is chosen same as the inverter switching time for study.

The estimator is tested for a step change in rotor resistance. The actual and estimated rotor resistance for step variation (24) is shown in Fig. 9(a). The sample weight evolution plot for step change is also shown in Fig. 9(b). It is understood that the network learns to estimate the rotor resistance. The weight and the rotor resistance are linearly related. The step change is the extreme case condition. It is used to show the capability of the proposed estimator to estimate R_r even in the extreme case condition.

But in the practical real time, the rotor resistance varies slowly. Accordingly, the proposed estimator is tested for trapezoidal variation (25) in the R_r and also with exponential variation Beguenane R *et al.* (1999) as in (26). The result obtained for trapezoidal variation and exponential variation is shown in the Fig. 9(c) and Fig. 9(d) respectively. The NN-MRAS tracks the variation in R_r for the various rotor resistance variation profile very well with good accuracy.

$$R_r(t) = \begin{cases} R_t,\text{nom} & 1 < 1.5\,\text{sec} \\ R_t,\text{nom} + \Delta R_t,\text{nom} & 1 < 1.5\,\text{sec} \end{cases} \quad (24)$$

$$R_r(t) = \begin{cases} R_r,\text{nom} & (t < 1\,\text{sec})\,\text{or}\,(t > 4\,\text{sec}) \\ \dfrac{t - (R_r,\text{nom})}{(R_r,\text{nom} + \Delta R_r,\text{nom}) - R_r,\text{nom}} & 1\,\text{sec} \le t \le 2\,\text{sec} \\ R_r,\text{nom} + \Delta R_r,\text{nom} & 2\,\text{sec} \le t \le 3\,\text{sec} \\ \dfrac{(R_r,\text{nom}) - t}{R_r,\text{nom} - (R_r,\text{nom} + \Delta R_r,\text{nom})} & 3\,\text{sec} \le t \le 4\,\text{sec} \end{cases} \quad (25)$$

$$R_t(t) = R_r,\text{nom} + (1 - e^{-1.2t}) \quad (26)$$

The estimated R_r value for various %changes in R_r is consolidated and presented in the Table 4 along with the steady state error for 100% and 50% load torque. It is found that the proposed estimator tracks, the change in R_r with good accuracy.

2.3 Adaptable Neural Network Based Rotor Resistance Estimator

The performance of the drive with and without a rotor resistance estimator is studied. The motor is operated with the speed of 148 rad/sec, torque of 7.5 Nm and rotor flux of 0.9 Wb. The step change in rotor resistance is effected at 1.5 sec. Without the R_r estimator, the rotor flux, torque and three phase stator current are shown in the Fig. 10 (a), Fig. (b), Fig. (c)

respectively. It is observed that without the rotor resistance estimator, the error in the rotor flux is found to be 16.66% and the actual flux deviates from the reference flux. The ripple in the machine torque is found to be 30.46% and oscillates about the load torque which is evident from Fig. 10(b). The sinusoidal shape of the three phase stator current gets distorted. This type of response is not desirable in high performance drives. With the rotor resistance estimator, the actual rotor flux tracks the reference flux with the error of 0.133% after about 0.4sec as soon as the step change in rotor resistance is applied at 1.5sec which is evident in Fig. 11(a). With the rotor resistance estimator, the ripple in the machine torque is reduced significantly to 3.382% which can be observed in Fig. 11 (b).

The sinusoidal shape of the current is maintained which can be observed from in Fig. 11(c). Hence, the performance of the CB-PWM-CMV based vector controlled IM drive is significantly enhanced with rotor resistance estimator.

Table 3. Effect of sampling time on the rotor resistance estimator for switching frequency 10kHz.

Sampling Time	Actual R_r (ohms)	Estimated R_r using Proposed NN-MRAS Scheme (ohms)	%Steady State Error
50μs	9.127	9.123	0.043826
100μs		9.114	0.142435
200μs		9.052	0.821738
300μs		8.958	1.851649
400μs		8.828	3.275994
500μs		8.657	5.149556

3. CONCLUSION

A carrier based PWM technique and Neural Network based rotor resistance estimator are proposed for the performance enhancement of induction motor drives. The CB-PWM-CMV technique is computationally less complex and gives ease in digital implementation as compared to space vector modulation technique. The CB-PWM-CMV technique is shown to improve the efficiency of the drive as compared to Sine-PWM. The CB-PWM-CMV technique is implemented on Spartan-6 FPGA processor and experimentally validated.

A neural Network based Model Reference Adaptive system in prediction mode is proposed for the rotor resistance estimation. The proposed NN-MRAS is shown to estimate R_r with good accuracy which is evident from Table 4. With rotor resistance estimator, the performance of the drive is significantly improved. Hence, it is concluded that the performance of the drive is enhanced significantly with CB-PWM-CMV and rotor resistance estimator.

(a)

(b)

(c)

(d)
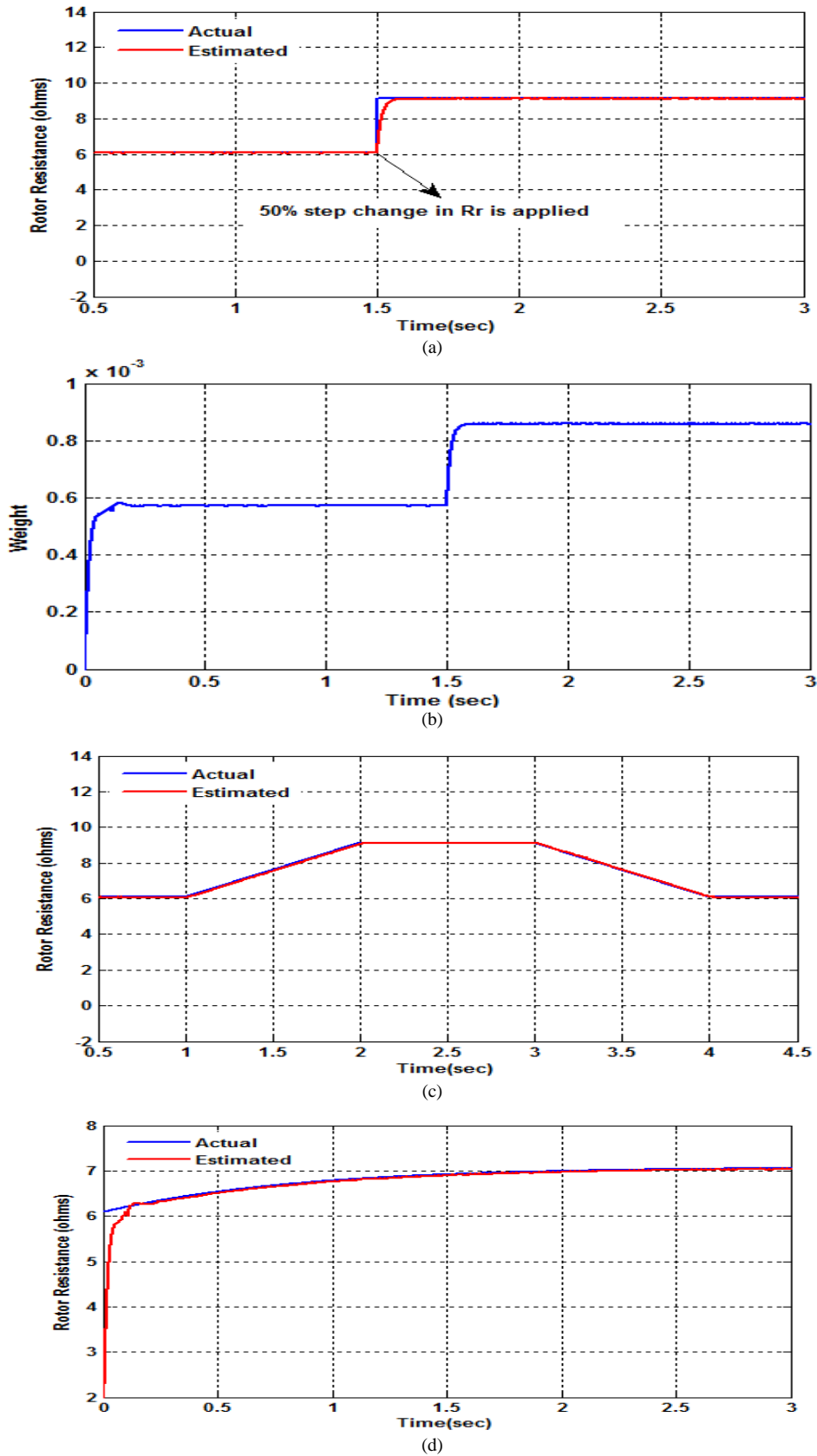
Figure 9. (a) Rotor resistance for step variation (b) Weight evolution plot for step variation (c) Rotor resistance for trapezoidal variation (d) Rotor resistance for exponential variation.
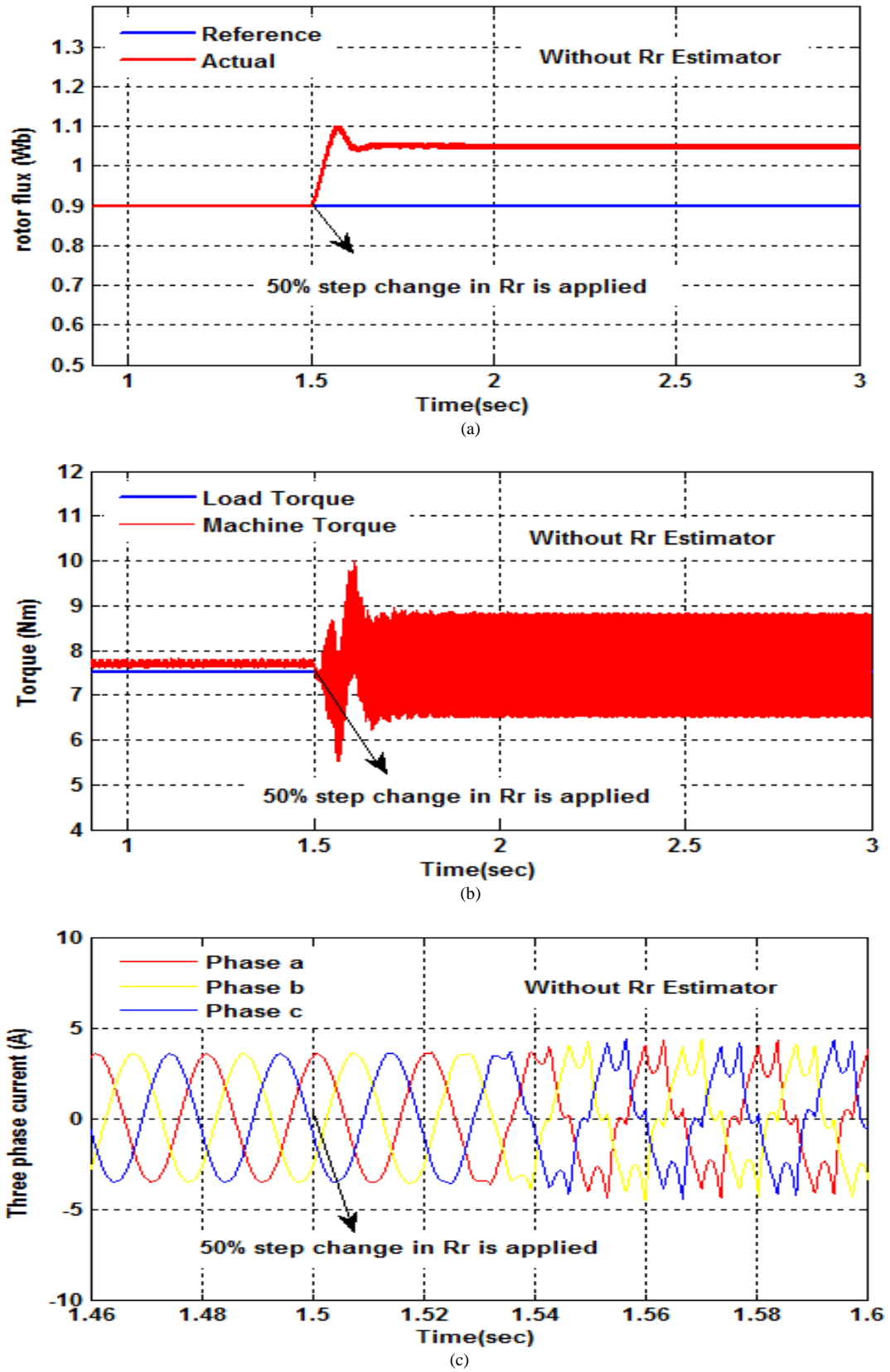
Figure 10. Without Rr Estimator: (a) Rotor Flux (b) Torque (c) Current.
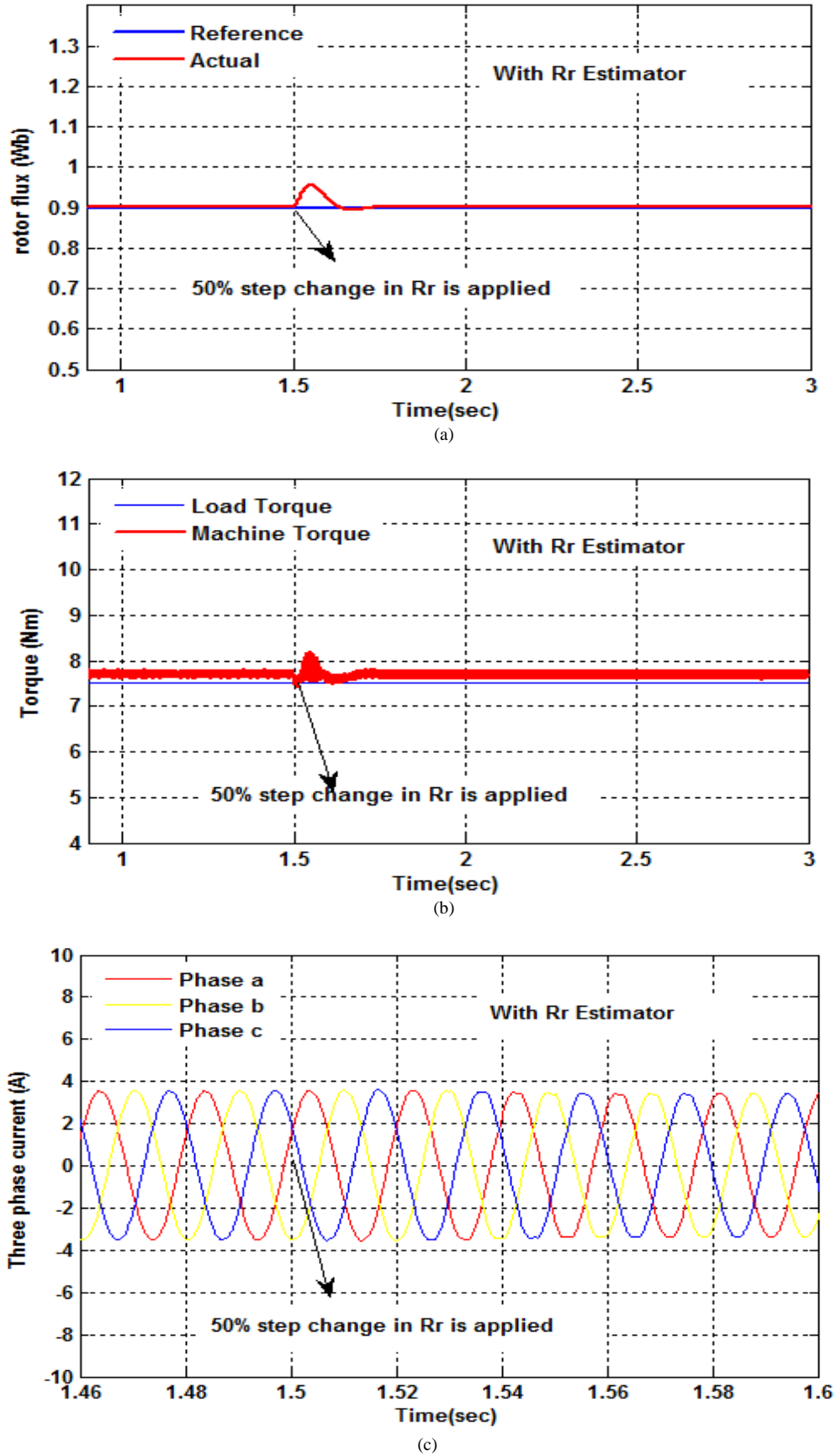
Figure 11. With Rr Estimator: (a) Rotor Flux (b) Torque (c) Current.

Table 4. Rotor resistance estimation using NN MRAS for various % changes in rotor resistance.

% Variation in R_r	Actual R_r (ohms)	100% Load Torque		50% Load Torque	
		Estimated R_r using Proposed NN-MRAS Scheme (ohms)	%Steady State Error	Estimated R_r using Proposed NN-MRAS Scheme (ohms)	%Steady State Error
10	6.69	6.672	0.328653	6.663	0.463101
20	7.30	7.284	0.246508	7.264	0.520405
30	7.91	7.983	-0.92288	7.889	0.265487
40	8.51	8.500	0.223031	8.487	0.375631
50	9.12	9.114	0.142435	9.098	0.317739
60	9.73	9.713	0.236237	9.711	0.256779
70	10.34	10.33	0.096712	10.32	0.193424
80	10.95	10.94	0.091324	10.92	0.273973
90	11.56	11.54	0.17301	11.53	0.259516
100	12.17	12.15	0.164339	12.14	0.246508

CONFILCT OF INTEREST

FUNDING

ACKNOWLEDGMENT

REFERENCES

Abdelkarim Ammar, Amor Bourek, Abdelhamid Benakcha (2017), Sensorless SVM-Direct torque control for induction motor drive using sliding mode observers. *Journal of Control, Automation mand Electrical Systems* 28(2): 189-201.

Ahmed A.Z.D (2014), Real-time implementation of full-order observer for speed sensorless vector control of induction motor drive. Journal of Control. *Automation and Electrical Systems* 25 (6): 639-648.

Beguenane R, Benbouzid M. E. H (1999), Induction motors thermal monitoring by means of rotor resistance identification. *IEEE Transactions on Energy Conversion* 14(3): 566-570.

Benchabane F, Titaouine A, Bennis O, Yahia K, Taibi D (2012), Direct field oriented control scheme for space vector modulated AC/DC/AC converter fed induction motor. *Frontiers in Energy* 6(2): 129-137.

Bimal K. Bose (2005), Modern power electronics and AC drives. Prentice Hall of India.

Chitra A, Himavathi S (2015), A modified neural learning algorithm for online rotor resistance estimation in vector controlled induction motor drives. *Frontiers in Energy* 9(1): 22-30.

Durgasukumar G, Pathak M.K (2012), Comparison of adaptive neuro-fuzzy-based space-vector modulation for two-level inverter. *Electrical Power and Energy Systems* 38: 9-19.

Govindasamy Renukadevi, Kalyanasundaram Rajambal (2014), Field programmable gate array implementation of space-vector pulse-width modulation technique for five-phase voltage source inverter. *IET Power Electronics* 7(2): 376-389.

Hannan M. A, Jamal Abd Ali, Azah Mohamed, Mohammad Nasir Uddin (2017), A random forest regression based space vector PWM inverter controller for the induction motor drive. *IEEE Transactions on Industrial Electronics* 64(4): 2689-2699.

Karanayil B, Rahman M.F and Grantham C (2007), Online stator and rotor resistance estimation scheme using artificial neural networks for vector controlled speed sensorless induction motor drive. *IEEE Transactions on Industrial Electronics* 54 (1): 167-176.

Keliang Zhou and Danwei Wang (2002), Relationship between space-vector modulation and three-phase carrier-based PWM: A comprehensive analysis. *IEEE Transactions on Industrial Electronics* 49

(1): 186-196.

Krishnan R (2007), Electric motor drives modeling, analysis and control. Prentice Hall of India.

Mahmoud Gaballah, Mohammed El-Bardini (2013), Low cost digital signal generation for driving space vector PWM inverter. *Ain Shams Engineering Journal* 4: 763-774.

Maurizio Cirrincione, and Marcello Pucci (2005), An MRAS-based sensorless high-performance induction motor drive with a predictive adaptive model. *IEEE Transactions on Industrial Electronics* 52(2): 532-551.

Peter Vas (1998), Sensorless vector and direct torque control. Oxford University Press.

Sabah V.S, Charles Baby T, Krishna Prabhakar Lall, Balamurugan M,Sarat Kumar Sahoo, Chitra A,Prabhakar, Karthikeyan, I. Jacob Raglend (2015), A simplified space vector pulse width modulation technique for multilevel inverter fed induction motor drive. IEEE International Conference on Circuit, Power and Computing Technologies (ICCPCT).

Shriwastava R.G, Daigavane M. B, Daigavane P. M (2016), Simulation analysis of three level diode clamped multilevel inverter fed PMSM drive using carrier based space vector pulse width modulation. (CB-SVPWM), Procedia Computer Science (Elsevier). 79: 616-623.

Srirattanawichaikul W, Kumsuwan Y, Premrudeepreechacharn S, Wu B (2011), Carrier-based PWM strategy for three-level neutral-point-clamped voltage source inverters. IEEE PEDS 2011, Singapore, 948-951.

Venkadesan A, Himavathi S and Muthuramalingam A (2016), A novel NN based rotor flux MRAS to overcome low speed problems for rotor resistance estimation in vector controlled IM drives. *Frontiers in Energy* 10(4): 382-392.

Venkadesan A, Himavathi S, Sedhuraman K, Muthuramalingam A (2017), Design and field programmable gate array implementation of cascade neural network based flux estimator for speed estimation in induction motor drives. *IET Electric Power Applications* 11(1): 121-131.

Witold P, Huynh V.K, Michael R.H (2017), Temperature rise estimation of induction motor drives based on loadability curves to facilitate design of electric powertrains. *IEEE Transactions on Industrial Informatics* 13(3): 985-994.

Appendix 1

Induction Motor Parameters: 3 phase, 4 poles, 1100W, 415V, 50Hz, 7.5Nm.

R_s	6.03Ω
R_r	6.085Ω
L_m	$0.4893H$
L_{sl}	$0.0138H$
L_{rl}	$0.0138H$
J	$0.011787kg.m^2$
B	$0.0027kg.m^2/s$